Turkish Journal of Electrical Engineering & Computer Sciences

http://journals.tubitak.gov.tr/elektrik/

Research Article

Turk J Elec Eng & Comp Sci
(2014) 22: 588 – 604

doi:10.3906/elk-1208-31

Bi input-extended Kalman filter-based speed-sensorless control of an induction machine capable of working in the field-weakening region

Remzi İNAN, Murat BARUT*
Department of Electrical and Electronics Engineering, Niğde University, Niğde, Turkey

Received: 09.08.2012 • **Accepted:** 19.12.2012 • **Published Online:** 21.03.2014 • **Printed:** 18.04.2014

Abstract: This study introduces a novel bi input-extended Kalman filter (BI-EKF)-based speed-sensorless direct vector control (DVC) of an induction motor (IM). The proposed BI-EKF-based estimator includes online estimations of the stator stationary axis components of the stator currents, $i_{s\alpha}$ and $i_{s\beta}$; stator stationary axis components of the rotor flux, $\varphi_{r\alpha}$ and $\varphi_{r\beta}$; rotor angular velocity, ω_m; stator resistance, R_s; rotor resistance, R_r; and load torque t_L, as well as the magnetizing inductance, L_m, by only supposing that the stator phase currents and voltages are measured. Thus, the speed-sensorless DVC of the IM with the inclusion of the proposed estimator is able to be perfectly operated at a wide speed range, varying from zero speed to beyond the rated/based speed under the extreme variations in R_s, R_r, t_L, and L_m. The simulations confirm the effectiveness of the proposed BI-EKF-based estimator and, consequently, the speed-sensorless DVC of the IM.

Key words: Induction motor, extended Kalman filter, rotor-stator resistance estimation, load torque estimation, magnetizing inductance estimation, sensorless control

1. Introduction

Highly efficient speed-sensorless control of induction motors (IMs) needs accurate estimations of ω_m, and/or flux at all speeds ranging from zero speed to very high speeds greater than the rated/based speed, which is known in the literature as the field-weakening region or operation. However, the speed-sensorless control of IMs still constitutes a big challenge [1–3], since those estimations are negatively affected by:

- Variations in R_s and R_r, which are caused by changing winding temperatures and frequencies.
- Variations in L_m, which occur in the field-weakening region because the flux reference has to be inversely reduced to below its rated value by increasing the velocity reference to beyond its rated value.
- Mechanical uncertainties, which particularly are variations in t_L, and friction.
- The difficulty at very low or zero speed in steady-state under no-load condition, which arises from the measured stator currents ceasing to carry on the rotor information since the electromagnetic induction between stator and rotor side of IM approaches zero, as well as noise and signal acquisition errors.

For the solution of the problems associated with the speed-sensorless control of IMs, a variety of estimation methods [4–8], which use deterministic IM models, have been very recently introduced in the literature; however,

*Correspondence: mbarut@nigde.edu.tr

they are especially sensitive to variations in R_s and/or R_r, together with variations in L_m. In addition to those, studies like those in [9–12] undertake performing both R_s and R_r estimations without L_m estimation. Nevertheless, the study in [9] does not demonstrate the estimation results of R_s and ω_m, together with R_r-estimation. In [10], R_s and ω_m estimations are sensitive to t_L variations, while R_r-estimation is performed by injecting a high-frequency signal on the magnetizing current command. The estimation algorithms in [11] and [12] are only executable whenever the speed-sensorless control system reaches its steady-state, which was declared by the authors. Attempts for including L_m-estimation into speed-sensorless estimation algorithms were also made in [13–16]; however, the algorithms in [13,15,16] were sensitive to variations in both R_s and R_r, while the study in [14] was affected by R_r variations.

In the literature, there is also another group of studies [17–19] based on novel extended Kalman filter (EKF) techniques, called switching EKF or braided EKF, using stochastic IM models for estimating R_s, R_r, and t_L, as well as ω_m; stator stationary components of the rotor (or stator) flux; and stator stationary components of the stator currents (also measured as output). In the switching or braided EKF techniques, 2 separate EKF algorithms developed by means of using 2 different IM models are consecutively operated to increase the number of states and parameter estimations that would be possible with a single standard EKF algorithm. If the consecutive operation is performed for each sampling time, T, then it is called braided EKF; otherwise, it is known as switching EKF. However, both switching and braided EKF require 2 separate EKF algorithms; this is not desired from the real-time implementation point of view since the cost of hardware platforms such as microprocessors, digital signal processors, and field programmable gate arrays increase with the increasing memory size/area required for embedding the software algorithm. A significant step forward in this sense is the method in [20,21], where the introduced bi input-EKF (BI-EKF) technique merges the consecutively operated 2 separate EKF algorithms into a single EKF algorithm by successively switching its input/terms associated with the 2 IM models; thus, the BI-EKF technique considerably reduces the memory requirement of both switching and braided EKF. Moreover, a novel version of the BI-EKF technique was recently introduced in [22], which estimates the total inertia, j_T, together with $i_{s\alpha}$, $i_{s\beta}$, $\varphi_{r\alpha}$, $\varphi_{r\beta}$, ω_m, R_s, R_r, and t_L by using the measured stator phase currents and voltages; therefore, it increases the number of estimated states and parameters compared to [20,21]. In other words, the novel version of the BI-EKF technique proposed in [22] estimates 5 common states ($i_{s\alpha}$, $i_{s\beta}$, $\varphi_{r\alpha}$, $\varphi_{r\beta}$, and ω_m) plus 2 different parameters (t_L and R_s or $1/j_T$ and R_r) at each sampling time, T. Considering Newton's equation of motion, $1/j_T$ is quite effective on estimation performances of position control systems in both transient and steady states, as well as on velocity control systems, but only in the transient state. Hence, the approach in [22] simultaneously estimates all of the mechanical variables of ω_m and t_L, including the viscous term, and $1/j_T$ together with the electrical ones of $i_{s\alpha}$, $i_{s\beta}$, $\varphi_{r\alpha}$, $\varphi_{r\beta}$, R_s, and R_r. Currently, none of studies using EKF developed for the speed-sensorless control of IM have taken L_m estimation into account, although a very few studies, which use a speed sensor/encoder based on EKF, as in [23–25], consider the field-weakening operation.

The major contribution of this study is to introduce a BI-EKF-based novel estimator embedded into the speed-sensorless direct vector control (DVC) of IMs using the novel version of BI-EKF technique in [22]. Different from [22], the proposed BI-EKF-based observer in this study provides the online estimations of $i_{s\alpha}$, $i_{s\beta}$, $\varphi_{r\alpha}$, $\varphi_{r\beta}$, ω_m, R_s, R_r, t_L, and L_m under the assumption that stator phase currents and voltages are available. Namely, the novel version of BI-EKF in this study performs the simultaneous estimation of the same group of states ($i_{s\alpha}$, $i_{s\beta}$, $\varphi_{r\alpha}$, $\varphi_{r\beta}$, and ω_m) plus t_L and R_s or L_m and R_r at each T. This achievement

is done using the newly introduced IM model with states of $i_{s\alpha}$, $i_{s\beta}$, $\varphi_{r\alpha}$, $\varphi_{r\beta}$, ω_m, R_r, and L_m in this manuscript. Thus, the introduced IM model and the previous one with states of $i_{s\alpha}$, $i_{s\beta}$, $\varphi_{r\alpha}$, $\varphi_{r\beta}$, ω_m, t_L, and R_s in [17,19–21] are combined in this study by utilizing the novel version of the BI-EKF technique in [22] in order to estimate all of the electrical variables of $i_{s\alpha}$, $i_{s\beta}$, $\varphi_{r\alpha}$, $\varphi_{r\beta}$, R_s, R_r, and L_m and the mechanical ones of ω_m and t_L, including the viscous term. L_m estimation is required to extend the speed operation range of the IM motor drive to the field-weakening region. Computer simulations performed under the challenging scenarios, including step-like variations of R_s, R_r, t_L, and L_m in a wide speed operation ranging from zero speed to above the rated speed, prove the effectiveness of the introduced BI-EKF-based estimator and thus of the speed-sensorless control system. From these points of view, it is the first known such study in the literature.

This paper is organized as follows: Section 1 introduces the problems and the literature associated with the speed-sensorless control of IMs. Section 2 reveals the IM models developed for the estimations of t_L and R_s or L_m and R_r, together with $i_{s\alpha}$, $i_{s\beta}$, $\varphi_{r\alpha}$, $\varphi_{r\beta}$, and ω_m. Sections 3 and 4 describe the BI-EKF-based novel estimator and the speed-sensorless DVC system with field-weakening operation, respectively. Section 5 presents the simulation results and observations. Section 6 gives the conclusions.

2. Extended mathematical models of the IM

The proposed BI-EKF algorithm in this study uses a rotor flux based on 2 different IM models: the first [17,19–21] is used for the estimations of $i_{s\alpha}$, $i_{s\beta}$, $\varphi_{r\alpha}$, $\varphi_{r\beta}$, ω_m, t_L, and R_s, while the other, which is first introduced in this study, is built up for $i_{s\alpha}$, $i_{s\beta}$, $\varphi_{r\alpha}$, $\varphi_{r\beta}$, ω_m, L_m, and R_r estimations. In the IM models, R_s, t_L, R_r, and L_m are evaluated as constant states by assuming that they have slow variation in time. Moreover, it is supposed that the stator phase current and voltages are measured. Under these considerations, the extended IM models in the discrete form, referred to as Model 1 and Model 2, are given in the following general form:

$$\underline{x}_{ei}(k+1) = \underline{f}_{ei}\left(\underline{x}_{ei}(k), \underline{u}_e(k)\right) + \underline{w}_{i1}$$

$$= \underline{A}_{ei}(\underline{x}_{ei}(k))\underline{x}_{ei}(k) + \underline{B}_e\underline{u}_e(k) + \underline{w}_{i1}, \tag{1}$$

$$\underline{Z}(k) = \underline{h}_{ei}(\underline{x}_{ei}(k)) + \underline{w}_{i2} \text{ (measurement equation)}$$

$$= \underline{H}_e\underline{x}_{ei}(k) + \underline{w}_{i2}. \tag{2}$$

Here, $i = 1$ or 2 represents each model; $\underline{x}_{ei}$ is the extended state vector for both models; $\underline{f}_{ei}$ is the nonlinear function of the states and inputs; $\underline{A}_{ei}$ is the system matrix; $\underline{u}_e$ is the control input vector; $\underline{B}_e$ is the input matrix; $\underline{w}_{i1}$ is the process noise; $\underline{h}_{ei}$ is the function of the outputs; $\underline{H}_e$ is the measurement matrix; and $\underline{w}_{i2}$ is the measurement noise.

Subject to the general expressions in Eqs. (1) and (2), the detailed state space representation of the extended IM models can be given as follows:

Model 1. The extended IM model used for t_L and R_s estimation. The matrices associated with this model [17,19–21], such as, $\underline{x}_{e1}$, $\underline{A}_{e1}$, $\underline{B}_{e1}$ and $\underline{u}_e$ are as follows:

$$\underline{x}_{e1} = \begin{bmatrix} i_{s\alpha}(k) & i_{s\beta}(k) & \varphi_{r\alpha}(k) & \varphi_{r\beta}(k) & \omega_m(k) & t_L(k) & R_s(k) \end{bmatrix}^T,$$

$$\underline{A}_{e1}\hat{=}\begin{bmatrix} 1-a_1R_s(k)-a_3 & 0 & a_4 & a_5\omega_m(k) & 0 & 0 & 0 \\ 0 & 1-a_1R_s(k)-a_3 & -a_5\omega_m(k) & a_4 & 0 & 0 & 0 \\ a_9 & 0 & 1-a_7 & -a_{10}\omega_m(k) & 0 & 0 & 0 \\ 0 & a_9 & a_{10}\omega_m(k) & 1-a_7 & 0 & 0 & 0 \\ -a_{11}\varphi_{r\beta}(k) & a_{11}\varphi_{r\alpha}(k) & 0 & 0 & 1 & -a_{12} & 0 \\ 0 & 0 & 0 & 0 & 0 & 1 & 0 \\ 0 & 0 & 0 & 0 & 0 & 0 & 1 \end{bmatrix},$$

$$\underline{B}_e=\begin{bmatrix} a_1 & 0 & 0 & 0 & 0 & 0 & 0 \\ 0 & a_1 & 0 & 0 & 0 & 0 & 0 \end{bmatrix}^T, \underline{u}_e=\begin{bmatrix} v_{s\alpha}(k) \\ v_{s\beta}(k) \end{bmatrix}.$$

The coefficients in Model 1 are as shown below:

$$a_1=\frac{T}{L_\sigma}, a_2=a_1\frac{L_m^2}{L_r}, a_3=a_2R_r^{'}, a_4=\frac{a_3}{L_m}, a_5=\frac{a_1L_mp_p}{L_r^{'}}, a_6=\frac{T}{L_r^{'}}, a_7=a_6R_r^{'}, a_8=a_6L_m, a_9=a_8R_r^{'},$$

$$a_{10}=p_pT, a_{11}=a_8\frac{1.5p_p}{J_T}, a_{12}=\frac{T}{J_T}, a_{13}=\frac{a_2}{L_m}, a_{14}=a_1R_s.$$

Model 2. The extended IM model proposed for L_m and R_r estimation in this study. The matrices in this model, $\underline{x}_{e2}$, $\underline{A}_{e2}$, $\underline{B}_{e2}$ and $\underline{u}_e$, are as follows:

$$\underline{x}_{e2}=[\ i_{s\alpha}(k) \quad i_{s\beta}(k) \quad \varphi_{r\alpha}(k) \quad \varphi_{r\beta}(k) \quad \omega_m(k) \quad L_m(k) \quad R_r(k)\ ]^T,$$

$$\underline{A}_{e2}\hat{=}\begin{bmatrix} 1-R_sf_1(k)-f_3(k) & 0 & f_3(k) & f_4(k)\omega_m(k) & 0 & 0 & 0 \\ 0 & 1-R_sf_1(k)-f_3(k) & -f_4(k)\omega_m(k) & f_3(k) & 0 & 0 & 0 \\ f_5(k) & 0 & 1-f_6(k) & -p_pT\omega_m(k) & 0 & 0 & 0 \\ 0 & f_5(k) & p_pT\omega_m(k) & 1-f_6(k) & 0 & 0 & 0 \\ -f_7(k)\varphi_{r\beta}(k) & f_7(k)\varphi_{r\alpha}(k) & 0 & 0 & 1 & -\frac{Tt_L}{J_T} & 0 \\ 0 & 0 & 0 & 0 & 0 & 1 & 0 \\ 0 & 0 & 0 & 0 & 0 & 0 & 1 \end{bmatrix},$$

$$\underline{B}_e=\begin{bmatrix} f_1(k) & 0 & 0 & 0 & 0 & 0 & 0 \\ 0 & f_1(k) & 0 & 0 & 0 & 0 & 0 \end{bmatrix}^T, \underline{u}_e=\begin{bmatrix} v_{s\alpha}(k) \\ v_{s\beta}(k) \end{bmatrix}.$$

The functions in Model 2 are as follows:

$$f_1(k)=\frac{T}{L_\sigma(k)}, f_2(k)=\frac{L_m(k)}{L_r(k)}, f_3(k)=f_1(k)f_2^2(k)R_r(k), f_4(k)=p_pf_1(k)f_2(k),$$

$$f_5(k)=Tf_2(k)R_r(k), f_6(k)=T\frac{R_r(k)}{L_r(k)}, f_7(k)=1.5p_p\frac{T}{J_T}f_2(k),$$

$$L_s(k) = L_r(k) = L_l + L_m(k),$$

$$L_\sigma(k) = L_s(k) - \frac{L_m^2(k)}{L_r(k)}.$$

In both IM models, p_p is the number of pole pairs; $L_\sigma = \sigma L_s$ is the stator transient inductance; $\sigma = 1 - \frac{L_m^2}{L_s L_r}$ is the leakage or coupling factor; L_s and L_r are the stator and rotor inductances, respectively; L_l is the stator (or rotor) leakage inductance; $v_{s\alpha}$ and $v_{s\beta}$ are stator stationary axis components of stator voltages; J_T is the total inertia of the IM and load; and T is the sampling time.

It is clear that:

- the only difference between Model 1 and Model 2 occurs from the constant states t_L and R_s in $\underline{x}_{e1}$ and L_m and R_r in $\underline{x}_{e2}$, respectively. Therefore, for more clarification, Model 1 and Model 2 are referred to as Model $t_L\&R_s$ and Model $L_m\&R_r$, respectively.
- the measurement noises, w_{12} and w_{22} in Eq. (2) are equal because $i_{s\alpha}$ and $i_{s\beta}$ are the measured states in both models.

3. Development of the BI-EKF-based novel estimator algorithm

The novel version of the BI-EKF technique introduced in [22] is adopted in this study in order to solve the simultaneous estimation problem of ω_m, R_s, and R_r, as well as $i_{s\alpha}$, $i_{s\beta}$, $\varphi_{r\alpha}$, $\varphi_{r\beta}$, t_L, and L_m, because it provides an increased number of states/parameter estimations compared to the conventional BI-EKF technique established in [20]. That is why this is the first time that the proposed BI-EKF-based estimator in this study presents the online estimations of R_s, t_L, R_r, and L_m, as well as all states required for the speed-sensorless control of IMs.

To build up the proposed estimator algorithm, first of all, standard EKF Eqs. (3a) through (3d) are defined as below.

$$\underline{F}_{ei}(k) = \left.\frac{\partial \underline{f}_{ei}(\underline{x}_{ei}(k), \underline{u}_e(k))}{\partial \underline{x}_{ei}(k)}\right|_{\hat{\underline{x}}_{ei}(k), \underline{u}_e(k)} \tag{3a}$$

$$\underline{N}_i(k) = \underline{F}_{ei}(k)\underline{P}_i(k)\underline{F}_{ei}^T(k) + \underline{Q}_i \tag{3b}$$

$$\underline{P}_i(k+1) = \underline{N}_i(k) - \underline{N}_i(k)\underline{H}_e^T(\underline{D}_\xi + \underline{H}_e\underline{N}_i(k)\underline{H}_e^T)^{-1}\underline{H}_e\underline{N}_i(k) \tag{3c}$$

$$\hat{\underline{x}}_{ei}(k+1) = \hat{\underline{f}}_{ei}(\hat{\underline{x}}_{ei}(k), \underline{u}_e(k)) + \underline{P}_i(k+1)\underline{H}_e^T D_\xi^{-1}(\underline{Z}(k) - \underline{H}_e\hat{\underline{x}}_{ei}(k)) \tag{3d}$$

Here, $\underline{F}_{ei}$ is the function used in the linearization of the nonlinear models in Eq. (1). $\underline{Q}_i$ is the covariance matrix of the system noise, namely the model error. $\underline{D}_\xi$ is the covariance matrix of the output noise, namely the measurement noise. $\underline{P}_i$ and $\underline{N}_i$ are the covariance matrix of the state estimation error and extrapolation error, respectively.

Later, the proposed estimator algorithm schematically demonstrated in Figure 1 is designed by considering Eqs. (3a) through (3d) and using the 3 remarks stated in [20,21].

Finally, the developed estimator algorithm is schematically demonstrated in Figure 1. As can be seen in Figure 1, the novel estimator unifies 2 separate EKF algorithms, which simultaneously estimate t_L and R_s

or L_m and R_r, together with $i_{s\alpha}$, $i_{s\beta}$, $\varphi_{r\alpha}$, $\varphi_{r\beta}$, and ω_m, by utilizing the measured stator phase currents and voltages in a single EKF algorithm by consecutively switching Input 1 and Input 2, which are derived from Model t_L&R_s and Model L_m&R_r, respectively. The consecutive operation is done for each sampling time, T. In other words, the online estimations of $i_{s\alpha}$, $i_{s\beta}$, $\varphi_{r\alpha}$, $\varphi_{r\beta}$, and ω_m, as well as t_L and R_s or L_m and R_r, are carried out during each T. At the end of each consecutive switching operation, the estimated L_m and R_r in the previous operation are considered constant parameters at Input 1 for the other group of estimations including t_L and R_s (or vice versa), while the estimations of $i_{s\alpha}$, $i_{s\beta}$, $\varphi_{r\alpha}$, $\varphi_{r\beta}$, and ω_m are updated to both Input 1 and Input 2. Moreover, $\underline{P}_i(k+1)$ is kept as $\underline{P}_i(k)$ for the usage of the next group of estimations.

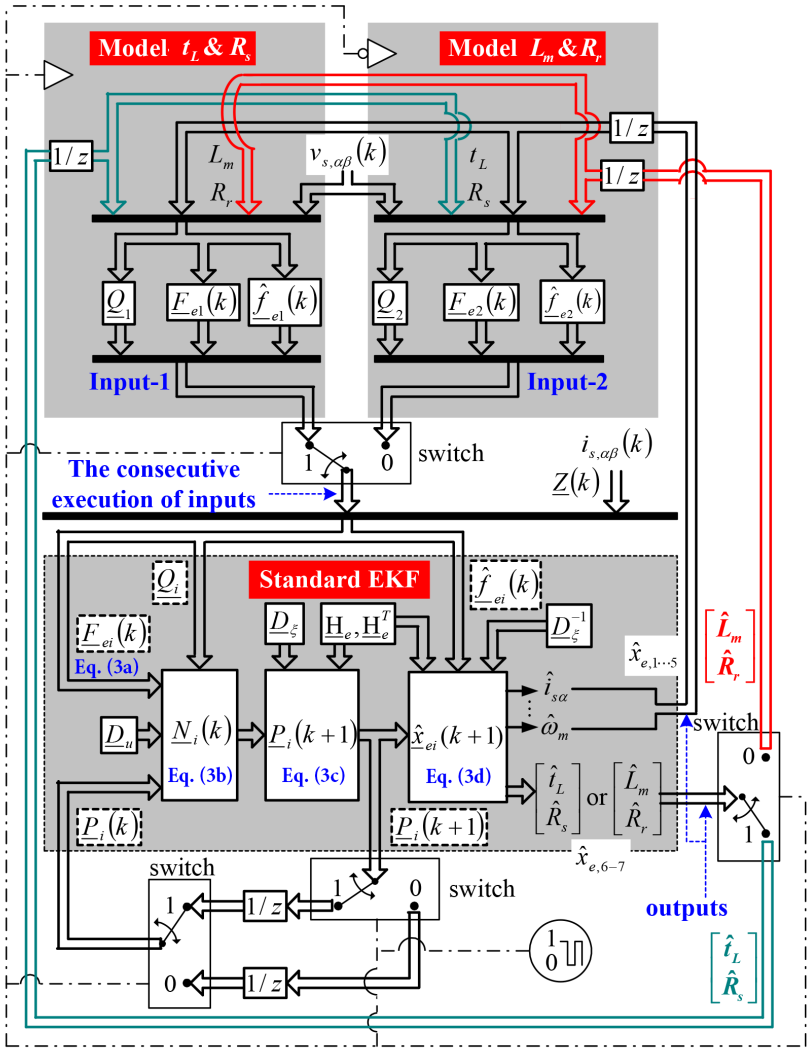

Figure 1. Schematic representation of the proposed estimator algorithm.

4. Speed-sensorless DVC system with field-weakening operation

The simulation setup for the performance test is given in Figure 2. Here, Figure 2a demonstrates the proposed BI-EKF-based rotor flux oriented speed-sensorless DVC system, including the field-weakening operation, which provides the speed control of the IM beyond its base speed, n_b (1500 rpm in this study). Figure 2b illustrates

the reference variations of n_m^r, t_L, $|\vec{\varphi}_r|^r$, R_r, R_s, and L_m for the estimation algorithm and control system. In the field weakening region, due to the voltage margin, the flux reference, $|\vec{\varphi}_r|^r$, has to be inversely decreased by increasing the speed reference, n_m^r; therefore, the magnetizing inductance is increased [13,14,26]. In Figure 2a, these relations, shown by a blue line, are mathematically expressed as below:

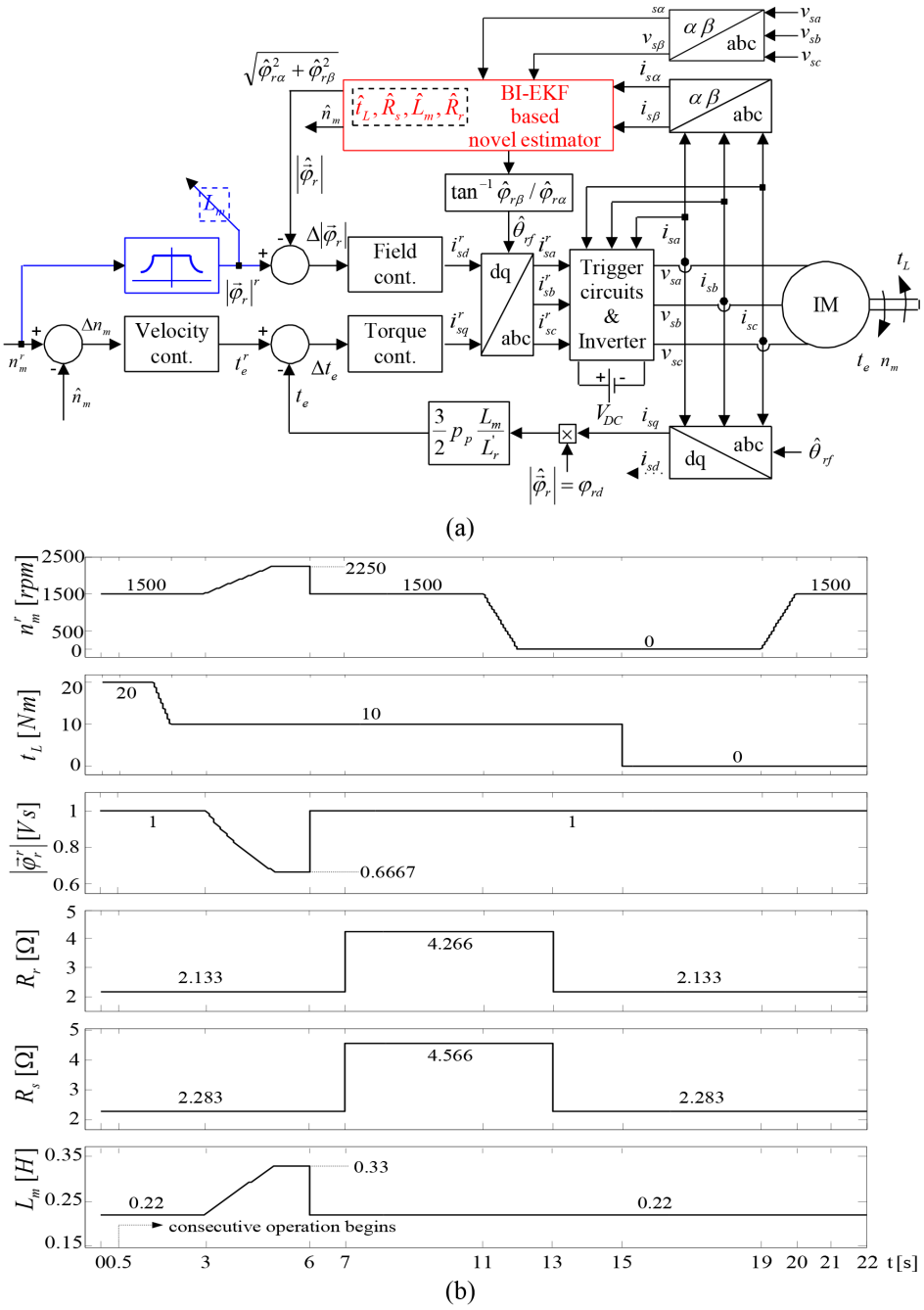

Figure 2. Simulation setup for performance test: a) the proposed BI-EKF-based rotor flux oriented speed-sensorless DVC system and b) reference variations of n_m^r, t_L, $|\vec{\varphi}_r|^r$, R_r, R_s, and L_m for the estimation algorithm and control system.

$$|\overrightarrow{\varphi_r}|^r = \frac{n_b}{n_m^r}\,|\varphi_r|^r_{rated} \text{ for } n_m^r > n_b, \tag{4a}$$

$$L_m = \frac{|\varphi_r|^r_{rated}}{|\overrightarrow{\varphi_r}|^r} L_{mn} \text{ for } n_m^r > n_b, \tag{4b}$$

where L_{mn} represents the constant L_m value obtained from the no-load and locked-rotor tests for $n_m^r \leq n_b$. On the other hand, in Figure 2a, $\hat{\theta}_{rf}$ is known as the field angle between the α-component of the stator stationary axis and d-component of the rotating axis, and the velocity, field, and torque controllers are in the form of conventional PIs.

5. Simulation results and observations

The IM used for the performance test of the BI-EKF-based novel estimator proposed in this study has the same rated parameters as that of the IM in past studies, as in [19,20], in order to make a fair comparison between the results in this study and those in [19,20], and these parameters are given below:

$$P[kW] = 3, f[Hz] = 50, J_T[kg.m^2] = 0.0183, \beta_T[N.m/(rad/s)] = 0, p_p = 2, V[V] = 380, I[A] = 6.9,$$

$$R_{sn}[\Omega] = 2.283, R_{rn}[\Omega] = 2.133, L_s[H] = L_r[H] = 0.2311, L_{mn}[H] = 0.22, n_{mn}[rpm] = 1430, t_{Ln}[N.m] = 20.$$

On the other hand, the values of all of the covariance matrices (P_i, Q_i, and D_ξ) used in the proposed BI-EKF-based estimator are considered as tuning parameters and are determined by trial-and-error in order to get the desired estimation performances, both in transient and in steady states. Finally, P_i, Q_i, and D_ξ, chosen in diagonal form for reducing computational complexity, are given as follows:

$$Q_1 = diag\{\ q_i \quad q_i \quad q_\varphi \quad q_\varphi \quad q_\omega \quad q_{t_L} \quad q_{R_s}\ \},$$

$$Q_2 = diag\{\ q_i \quad q_i \quad q_\varphi \quad q_\varphi \quad q_\omega \quad q_{L_m} \quad q_{R_r}\ \},$$

$$P_i = diag\{\ p \quad p \quad p \quad p \quad p \quad p \quad p\ \}, D_\xi = diag\{\ d \quad d\ \},$$

where

$$q_i = 10^{-9}A^2, q_\varphi = 10^{-9}(V.s)^2, q_\omega = 10^{-4}(rad/s)^2, q_{t_L} = 10^{-4}(N.m)^2,$$

$$q_{R_s} = 10^{-5}\Omega^2, q_{L_m} = 10^{-6}H^2, q_{R_r} = 10^{-5}\Omega^2, p = 9, d = 10^{-6}V^2.$$

According to the literature on the speed-sensorless control of IMs, this is the first time that the proposed estimator and thus the speed sensorless control of IMs have been tested under the variations in R_s, R_r, t_L, and L_m in a wide-speed range, including both zero speed and beyond the rated speeds. These challenging variations are shown in Figure 2b. Finally, the simulation results obtained from the proposed BI-EKF-based estimator and the speed-sensorless control system without the need for a white noise addition to the measured states are presented in Figures 3a–3g, which demonstrate the variations of $\hat{n}_m$, $\hat{t}_L$, $\hat{R}_r$, $\hat{R}_s$, $\hat{L}_m$, $\left|\widehat{\overrightarrow{\varphi}}_r\right| = \sqrt{\varphi_{r\alpha}^2 + \varphi_{r\beta}^2}$, and $\hat{\theta}_{rf} = \tan^{-1}\hat{\varphi}_{r\beta}/\hat{\varphi}_{r\alpha}$, respectively. Figures 4a–4h, which refer to the estimation and tracking errors associated with Figures 3a–3g, show the variations of $e_{n_m} = n_m - \hat{n}_m$, $\Delta n_m = n_m^r - \hat{n}_m$, $e_{L_m} = L_m - \hat{L}_m$, $e_{t_L} = t_L - \hat{t}_L$, $e_{R_s} = R_s - \hat{R}_s$, $e_{\overrightarrow{\varphi}_r} = |\overrightarrow{\varphi}_r| - \left|\widehat{\overrightarrow{\varphi}}_r\right|$, and $\Delta\,|\overrightarrow{\varphi}_r| = |\overrightarrow{\varphi}_r|^r - \left|\widehat{\overrightarrow{\varphi}}_r\right|$, respectively. In Figures 3

and 4, T is 100 μs; $\wedge$ denotes the estimated state or parameter; and errors, $e_{(.)}$, are denoted as the deviation between the actual and the estimated variable. Each of the zoom-in or dashed-line boxes in Figure 4 is used to demonstrate how accurately the estimations shown in Figure 3 converge to their real values indicated in Figure 2b.

Considering Figure 2b, the simulations basically consist of the next 5 challenging operations.

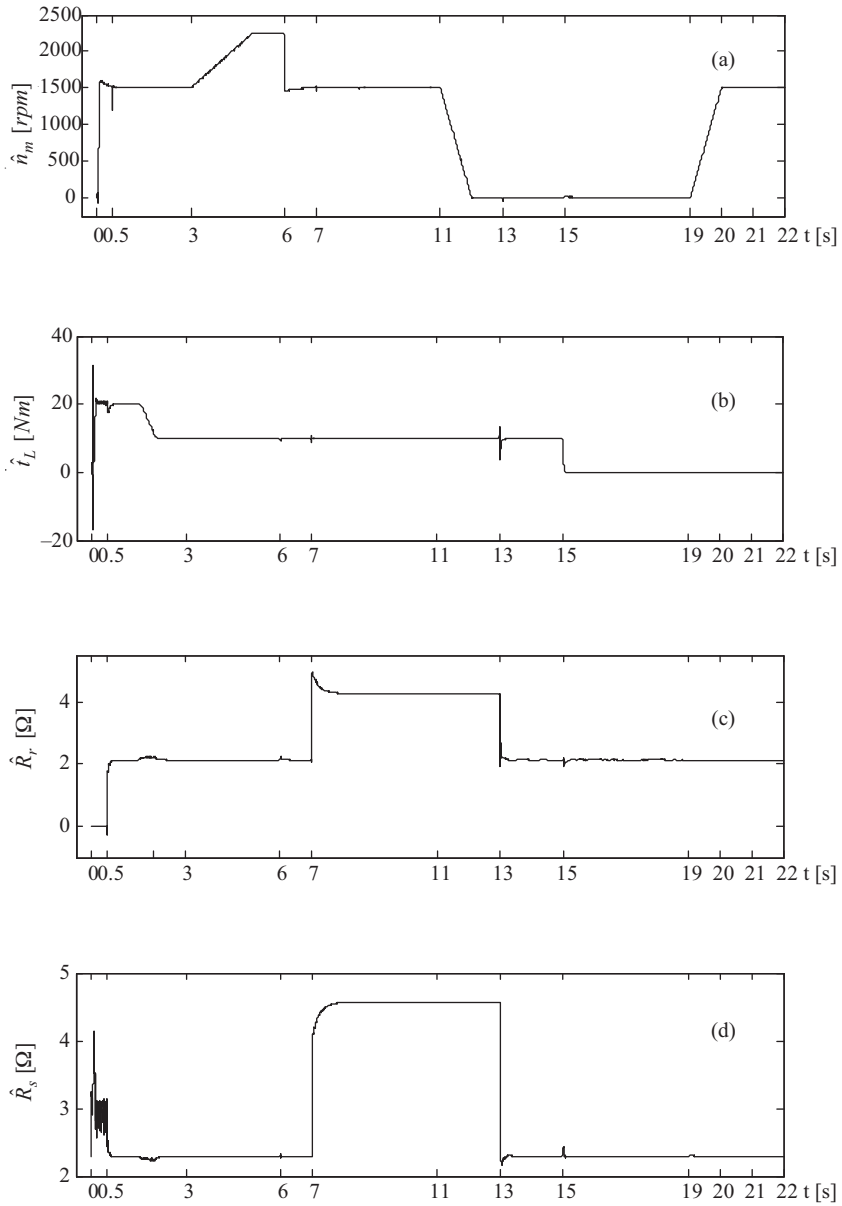

Figure 3. Simulation results for the proposed BI-EKF-based estimator and the DVC system: a) variation of $\hat{n}_m$, b) variation of $\hat{t}_L$, c) variation of $\hat{R}_r$, d) variation of $\hat{R}_s$, e) variation of $\hat{L}_m$, f) variation of $\left|\widehat{\overrightarrow{\varphi}}_r\right| = \sqrt{\varphi_{r\alpha}^2 + \varphi_{r\beta}^2}$, and g) variation of $\hat{\theta}_{rf} = \tan^{-1} \hat{\varphi}_{r\beta}/\hat{\varphi}_{r\alpha}$.

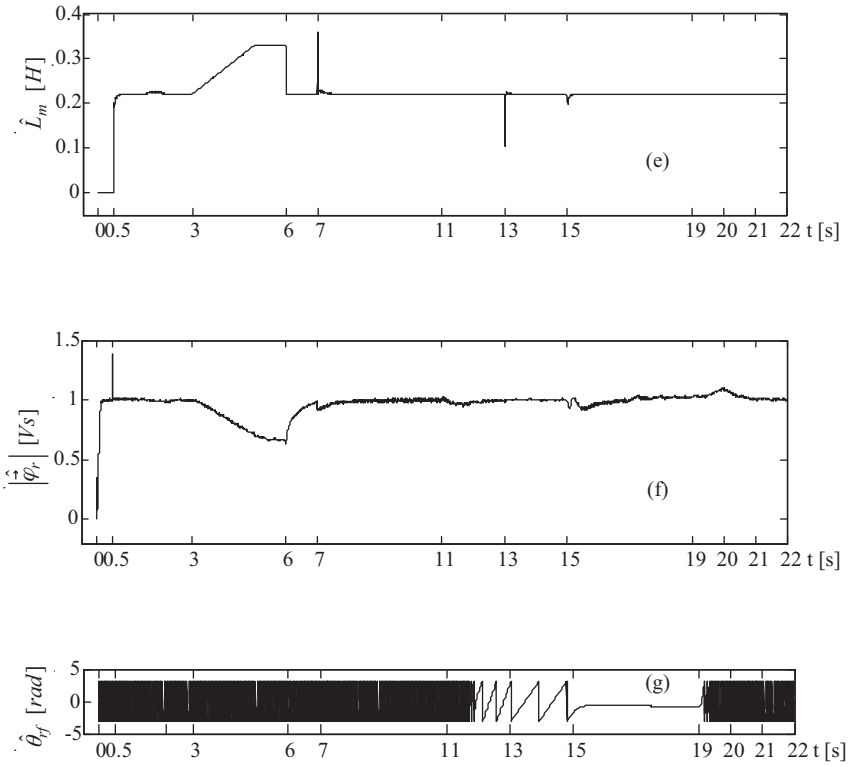

Figure 3. Continued.

5.1. Initialization and moving to the consecutive operation ($0 \leq t \leq 1.5$ s)

During this operation, the IM freely speeds up to the based speed, $n_b = 1500$ rpm, under the rated load torque, $t_{Ln} = 20$ Nm. Here, the BI-EKF-based novel estimator begins the consecutive operation at 0.5 s after the initialization stage, in which it is given a start using only Model $t_L\&R_s$ with incorrect $R_r = 0.5 \times R_{rn}$ and the correct $L_m = L_{mn}$; the initial values of $\hat{i}_{s\alpha}$, $\hat{i}_{s\beta}$, $\hat{\varphi}_{r\alpha}$, $\hat{\varphi}_{r\beta}$, $\hat{\omega}_m$, $\hat{R}_s$, and $\hat{t}_L$ are also taken as 0 at the beginning of the initialization stage. The initial values of the states and parameters in the introduced BI-EKF are logical:

- since a speed below or equal to n_b results in constant-rated L_m (L_{mn}).
- because of using an incorrect R_r value. The R_r value calculated from the results associated with the no-load and locked-rotor tests is only valid for rated frequency and load conditions, especially in a squirrel cage-type IM.

As seen from Figures 3–4, for the time range of $0 \leq t \leq 0.5$ s, the estimations are still stable, but include some errors due to the incorrect R_r value; however, these errors quickly go to 0 after the proposed BI-EKF-based estimator starts the successive operation at 0.5 s by utilizing the 2 inputs derived from Model $t_L\&R_s$ and Model $L_m\&R_r$. Therefore, it is concluded that the proposed BI-EKF estimator can tolerate the incorrect R_r value while performing the estimations based on Model $t_L\&R_s$. Moreover, even though the initial values of $\hat{R}_s$, $\hat{R}_r$, $\hat{t}_L$, and $\hat{L}_m$ are taken as 0, all of the estimations rapidly converge to real ones during $0 \leq t \leq 1.5$ s; these realities can be discovered by inspecting Figures 3b–3e and 4c–4f at 0 s for $\hat{R}_s$ and $\hat{t}_L$ and at 0.5 s for $\hat{R}_r$ and $\hat{L}_m$.

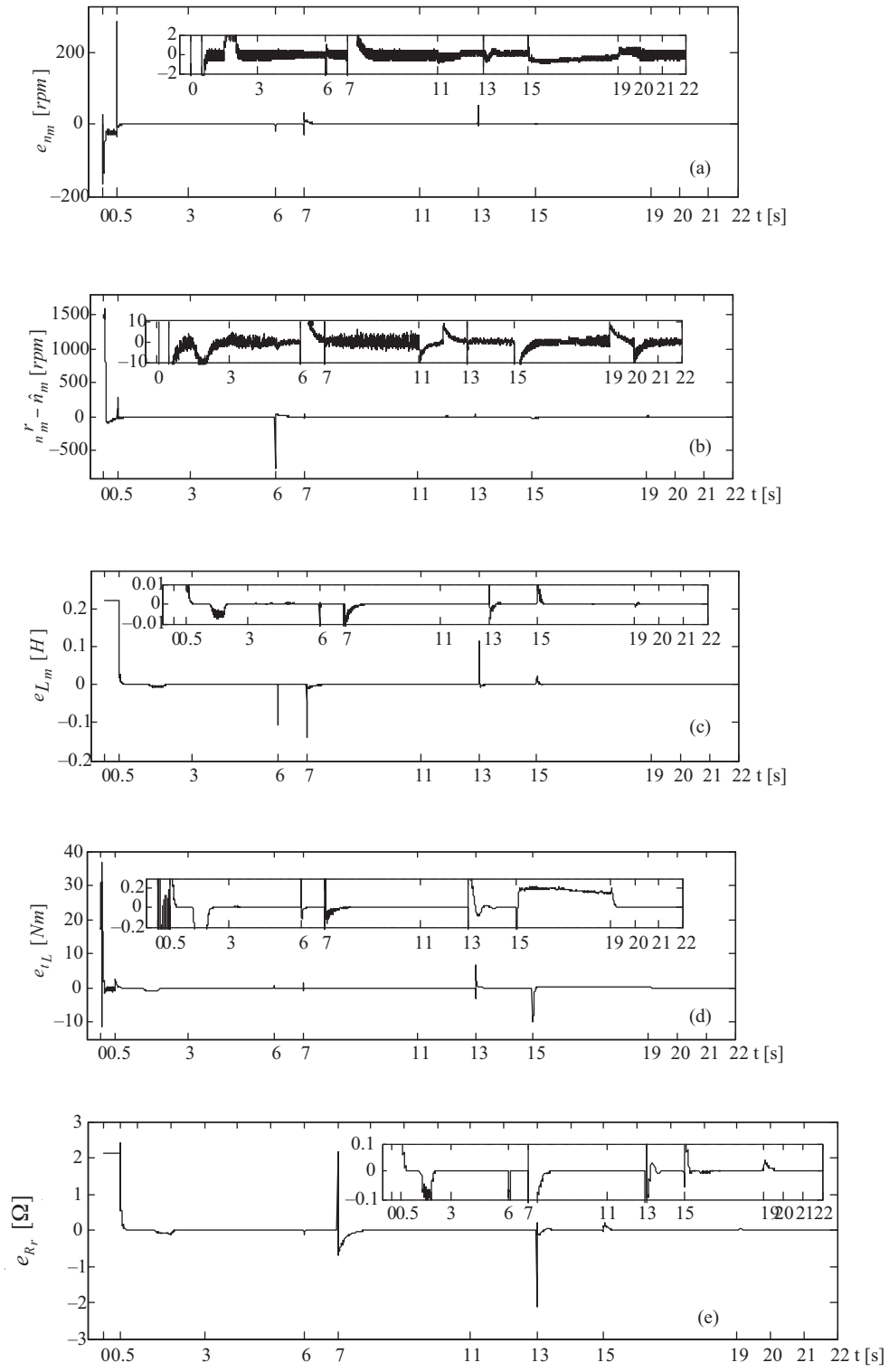

Figure 4. Simulation results for the estimation and tracking errors: a) variation of $e_{n_m} = n_m - \hat{n}_m$, b) variation of $\Delta n_m = n_m^r - \hat{n}_m$, c) variation of $e_{L_m} = L_m - \hat{L}_m$, d) variation of $e_{t_L} = t_L - \hat{t}_L$, e) variation of $e_{R_r} = R_r - \hat{R}_r$, f) variation of $e_{R_s} = R_s - \hat{R}_s$, g) variation of $e_{\overrightarrow{\varphi}_r} = |\overrightarrow{\varphi}_r| - \left|\widehat{\overrightarrow{\varphi}}_r\right|$, and h) variation of $\Delta\,|\overrightarrow{\varphi}_r| = |\overrightarrow{\varphi}_r|^r - \left|\widehat{\overrightarrow{\varphi}}_r\right|$.

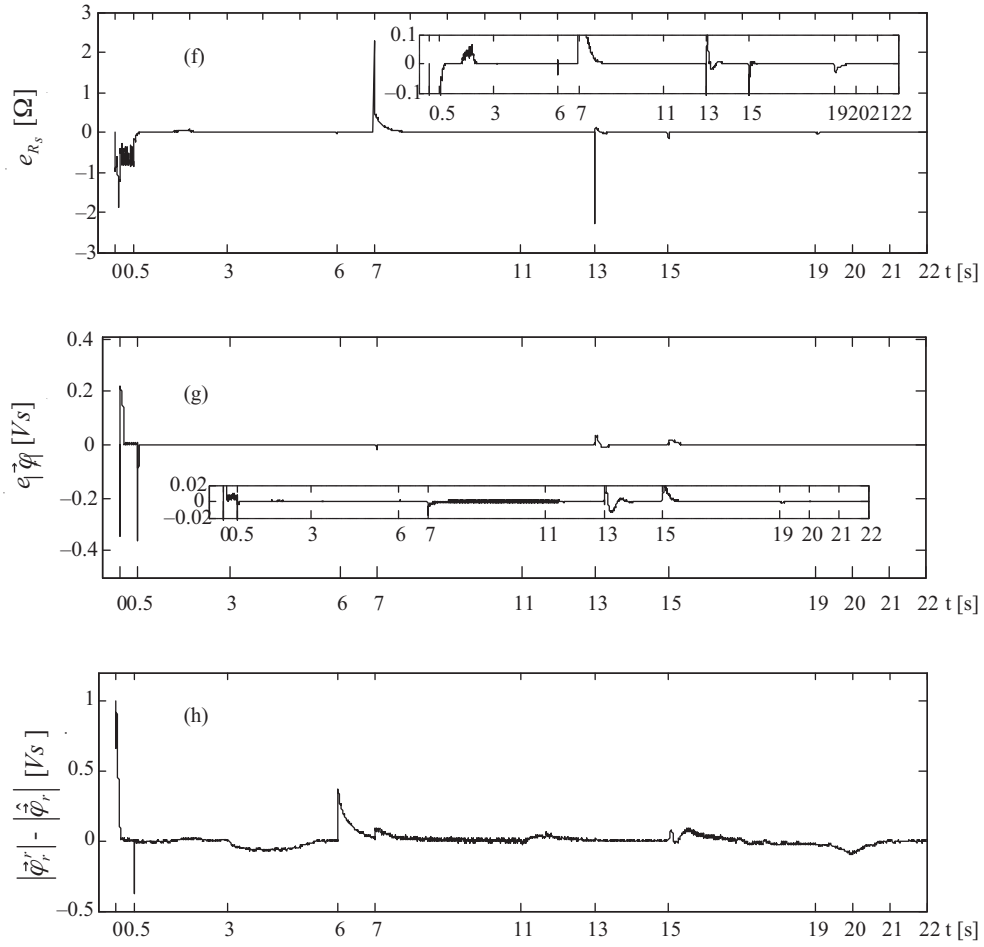

Figure 4. Continued.

5.2. The field weakening operation ($3 \leq t \leq 6\,s$)

In this region, the speed-sensorless drive is operated by reducing $|\overrightarrow{\varphi_r}|^r$ to below $|\varphi_r|^r_{rated}$ for $n^r_m > n_b = 1500\ rpm$, and the reduced $|\overrightarrow{\varphi_r}|^r$ causes increases in L_m, as demonstrated in Figure 2b, for the time range of $3 \leq t \leq 5\ s$. In addition to these constantly small variations during $3 \leq t \leq 5\ s$, step-like variations at $0.5\ s$ and $6\ s$ are generated to challenge the proposed BI-EKF algorithm. Those challenging variations are precisely identified by the proposed estimator, as seen in Figures 3e and 4c. Moreover, n_m and $\overrightarrow{\varphi_r}$ are accurately estimated and well regulated by the speed-sensorless control system under these variations, as shown in Figures 4a, 4b, 4g, and 4h. The obtained results confirm that the field-weakening operation can be performed in a very good way by the proposed BI-EKF-based estimator without knowledge of the IM's magnetizing curve obtained from additional attempts, as described in [3], which was mostly done in previous studies, such as in [13–15].

5.3. The linear and step-like variations in t_L ($1.5 \leq t \leq 20\,s$)

In this interval, it is desired to test if the proposed BI-EKF algorithm tracks linear t_L variations occurring in the time range of $1.5 \leq t \leq 2\ s$ and the step-like t_L variations starting at $15\ s$, as shown in Figure 2b.

Although t_L is defined as a constant state in Model $t_L\&R_s$, the proposed estimator algorithm exactly follows the real t_L, and the estimation error immediately converges to 0 after the variations, as seen from Figures 3b and 4d. The proposed algorithm is capable of identifying the viscous friction term $\beta_T\omega_m$ in $\hat{t}_L$, as in [19,20,22], but this is not shown here.

5.4. $\mathbf{R_s}$ and $\mathbf{R_r}$ variations at high/zero speed under load torque ($\mathbf{7 \leq t \leq 13\,s}$)

In these experiments, R_s and R_r are stepped up to $2 \times R_{sn}$ and $2 \times R_{rn}$, respectively, at the same time (at 7 s), while the IM is running at 1500 rpm under $t_{Ln} = 20$ Nm. Later, both R_s and R_r are instantly decreased to R_{sn} and R_{rn}, respectively, at 13 s under the zero speed case, in which the IM is loaded to $t_{Ln} = 10$ Nm. In spite of these challenging R_s and R_r variations taking place together at both high and zero speeds, the proposed estimator reaches the actual values of both R_s and R_r in a very short time, as shown in Figures 3c, 3d, 4e, and 4f.

5.5. Zero speed under no-load conditions and return to the base speed ($\mathbf{15 \leq t \leq 22\,s}$)

In the time interval of $15 \leq t \leq 19\ s$, a well-known big challenge exists for the IM state and parameter estimations since $\hat{\theta}_{rf} = \tan^{-1}\frac{\hat{\varphi}_{r\beta}}{\hat{\varphi}_{r\alpha}}$ becomes constant, as seen Figure 3g. Thus, no induction occurs from the stator side to the rotor one, which means that the measured stator currents stop conveying the rotor-side information. Nevertheless, the proposed estimator presents very acceptable results, which were done in another study [20]. This is because of:

- using the equation of motion, which improves the estimation performance at zero speed under no-load conditions [20].

- exploiting the model and measurement noise inherent to EKFs, which causes the persistence of excitation required for convergence in the steady state, especially at low and zero speeds [18].

During $19 \leq t \leq 22\ s$, it is desired to show that the proposed BI-EKF algorithm is able to estimate all states and parameters, even after the worst case for the IM state and parameter estimation in the time range of $15 \leq t \leq 19\ s$.

On the other hand, other groups of simulations are also performed by both the proposed estimator in this study and the estimator developed in a recently published study [20] under the same reference variations in order to make comparisons between them. The reference variations are shown in Figure 5a, while the estimation errors for both estimators are demonstrated in Figures 5b–5e, which depict the variations of $e_{n_m} = n_m - \hat{n}_m$, $e_{R_r} = R_r - \hat{R}_r$, $e_{t_L} = t_L - \hat{t}_L$, and $e_{R_s} = R_s - \hat{R}_s$, respectively. As can be clearly seen from Figure 5, the estimator developed in [20] has undesired errors on the estimated states and parameters in the interval of $4 \leq t \leq 7\ s$, where the variations in L_m occur since it does not take L_m-estimation into account, together with $i_{s\alpha}$, $i_{s\beta}$, $\varphi_{r\alpha}$, $\varphi_{r\beta}$, ω_m, R_s, R_r, and t_L. Those errors also increase with the increasing n_m and/or t_L, or vice versa. Thus, the presented results in Figures 5b–5e validate the superiority of the proposed estimator in this study over that in [20]; thus, they call for the L_m-estimation as well as $i_{s\alpha}$, $i_{s\beta}$, $\varphi_{r\alpha}$, $\varphi_{r\beta}$, ω_m, R_s, R_r, and t_L.

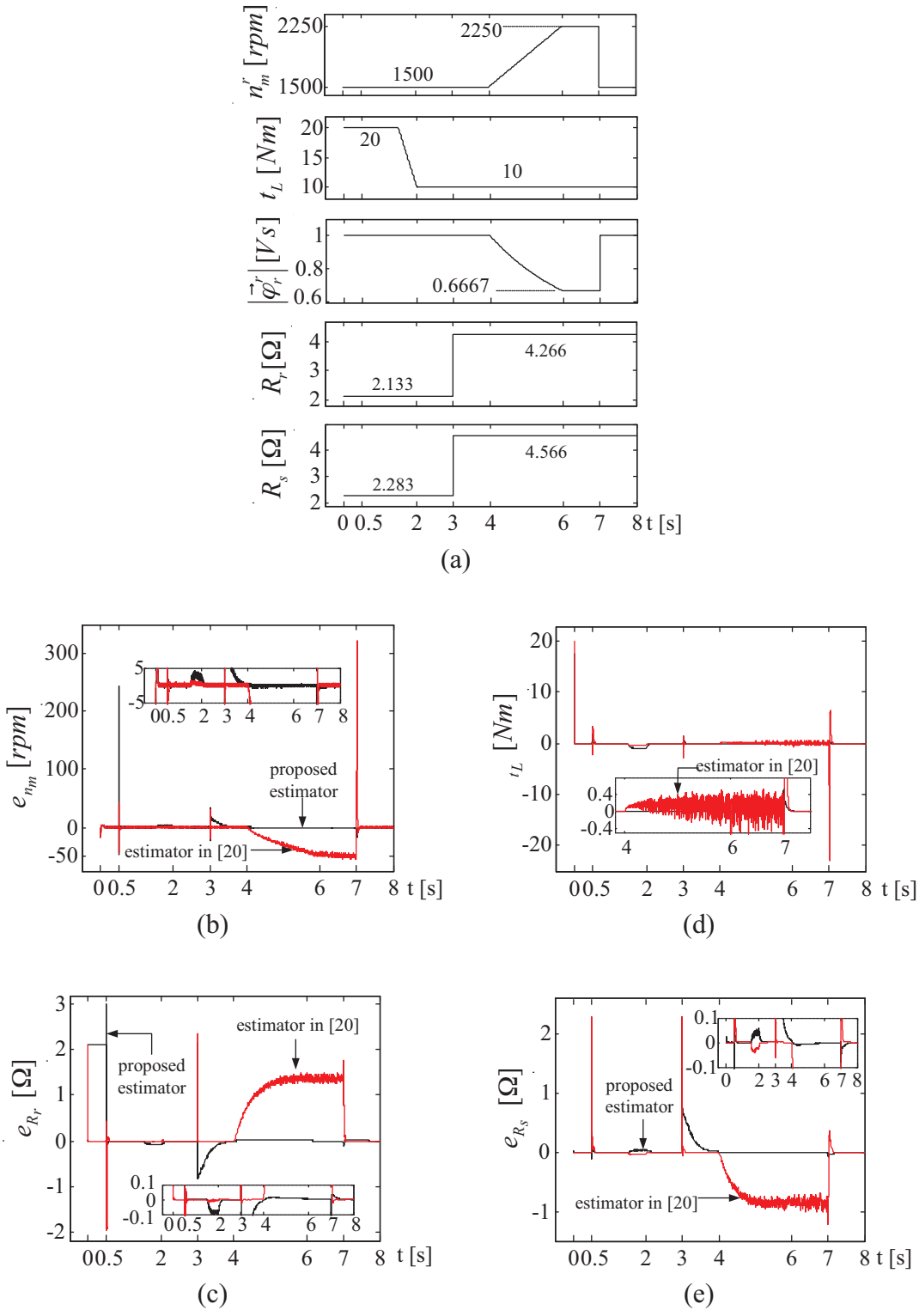

Figure 5. Comparative simulation results for the proposed observer and the observer in [20]: a) variations of n_m^r, t_L, $|\vec{\varphi}_r|^r$, R_r, R_s, and L_m for the comparison test; b) variations of $e_{n_m} = n_m - \hat{n}_m$; c) variations of $e_{R_r} = R_r - \hat{R}_r$; d) variations of $e_{t_L} = t_L - \hat{t}_L$; and e) variations of $e_{R_s} = R_s - \hat{R}_s$.

6. Conclusion

In this study, a novel BI-EKF-based estimator, which is capable of the online estimating of $i_{s\alpha}$, $i_{s\beta}$, $\varphi_{r\alpha}$, $\varphi_{r\beta}$, ω_m, R_s, R_r, t_L, and L_m by only measuring the stator phase currents and voltages, was designed, and it was inserted into the speed-sensorless DVC of IMs for performance tests, which were made for the wide speed range extending from zero speed to beyond the rated/based speed under the challenging variations in R_s, R_r, t_L, and L_m. These achievements are first obtained in this study according to the current literature associated with the speed-sensorless control of IMs. The simulation-based experiments prove the benefit of the proposed BI-EKF-based algorithm and therefore of the speed-sensorless control system of the IM compared with previous studies, such as [20]. The proposed estimator also has theoretically interesting and practically significant properties, as stated below:

- It overcomes the simultaneous estimation problem of R_s, R_r, and L_m, together with all of the required states for the speed-sensorless velocity control of IMs under both zero and rated load torque.
- It considerably reduces the memory area required for the estimation algorithm, as well as the design time and stages, because it merges 2 separate EKF algorithms into a single EKF, as defined in Section 3, compared to its counterpart to be performed by the braided [17,18] or the switching [19] EKF techniques.

However, the optimal calculation of the system covariance matrix, Q_i, is still a well-known problem to be solved in the literature. Therefore, future studies should be done for the solution of this issue. From another point of view, the speed-sensorless control issues of IMs are still open to research and are very attractive in the literature, and the main problems and other topics related to the speed-sensorless control of IMs can be usefully discovered by inspecting [27–29].

Acknowledgment

This work was supported by the Scientific and Technological Research Council of Turkey (TÜBİTAK) under research grant EEEAG-108E187.

References

[1] J. Holtz, "Sensorless control of induction machines—with or without signal injection?", IEEE Transactions on Industrial Electronics, Vol. 53, pp. 7–30, 2006.

[2] J.W. Finch, D. Giaouris, "Controlled AC electrical drives", IEEE Transactions on Industrial Electronics, Vol. 55, pp. 481–491, 2008.

[3] H.A. Toliyat, E. Levi, M. Raina, "A review of RFO induction motor parameter estimation techniques", IEEE Transactions on Energy Conversion, Vol. 18, pp. 271–283, 2003.

[4] T. Orlowska-Kowalska, M. Dybkowski, "Stator-current-based MRAS estimator for a wide range speed-sensorless induction-motor drive", IEEE Transactions on Industrial Electronics, Vol. 57, pp. 1296–1308, 2010.

[5] M. Hajian, J. Soltani, G.A. Markadeh, S. Hosseinnia, "Adaptive nonlinear direct torque control of sensorless IM drives with efficiency optimization", IEEE Transactions on Industrial Electronics, Vol. 57, pp. 975–985, 2010.

[6] I. Vicente, A. Endemano, X. Garin, M. Brown, "Comparative study of stabilising methods for adaptive speed sensorless full-order observers with stator resistance estimation", IET Control Theory & Applications, Vol. 4, pp. 99–1004, 2010.

[7] M.S. Zaky, M. Khater, H. Yasin, S.S. Shokralla, "Very low speed and zero speed estimations of sensorless induction motor drives", Electric Power Systems Research, Vol. 80 pp. 143–151, 2010.

[8] A. Paladugu, B.H. Chowdhury, "Sensorless control of inverter-fed induction motor drives", Electric Power Systems Research, Vol. 77, pp. 619–629, 2007.

[9] B. Karanayil, M.F. Rahman, C. Grantham, "Online stator and rotor resistance estimation scheme using artificial neural networks for vector controlled speed sensorless induction motor drive", IEEE Transactions on Industrial Electronics, Vol. 54, pp. 167–176, 2007.

[10] H. Tajima, G. Guidi, H. Umida, "Consideration about problems and solutions of speed estimation method and parameter tuning for speed-sensorless vector control of induction motor drives", IEEE Transactions on Industry Applications, Vol. 38, pp. 1282–1289, 2002.

[11] I.J. Ha, S.H. Lee, "An online identification method for both stator-and rotor resistances of induction motors without rotational transducers", IEEE Transactions on Industrial Electronics, Vol. 47, pp. 842–853, 2000.

[12] L. Zhen, L. Xu, "Sensorless field orientation control of induction machines based on a mutual MRAS scheme", IEEE Transactions on Industrial Electronics, Vol. 45, pp. 824–831, 1998.

[13] T. Orlowska-Kowalska, G. Tarchala, M. Dybkowski, "Sliding-mode control and sliding-mode speed observer extended with additional magnetizing reactance estimator for induction motor drives", ELECTRIMACS Conference Records, 2011 (on CD).

[14] M.S. Zaky, M.M. Khater, S.S. Shokralla, H.A. Yasin, "Wide-speed-range estimation with online parameter identification schemes of sensorless induction motor drives", IEEE Transactions on Industrial Electronics, Vol. 56, pp. 1699–1707, 2009.

[15] E. Levi, M. Wang, "A speed estimator for high performance sensorless control of induction motors in the field weakening region", IEEE Transactions on Power Electronics, Vol. 17, pp. 365–378, 2002.

[16] J.S. Choi, Y.S. Han, Y.S. Kim, "A new speed estimation scheme of the induction motor considering the flux saturation, IEEE Transactions on Magnetics, Vol. 36, pp. 3595–3598, 2000.

[17] M. Barut, S. Bogosyan, M. Gokasan, "Experimental evaluation of braided EKF for sensorless control of induction motors", IEEE Transactions on Industrial Electronics, Vol. 55, pp. 620–632, 2008.

[18] S. Bogosyan, M. Barut, M. Gokasan, "Braided extended Kalman filters for sensorless estimation in induction motors at high-low/zero speed", IET Control Theory & Applications, Vol. 1, pp. 987–998, 2007.

[19] M. Barut, S. Bogosyan, M. Gokasan, "Switching EKF technique for rotor and stator resistance estimation in speed sensorless control of IMs", Energy Conversion and Management, Vol. 48, pp. 3120–3134, 2007.

[20] M. Barut, "Bi input-extended Kalman filter based estimation technique for speed-sensorless control of induction motors", Energy Conversion and Management, Vol. 51, pp. 2032–2040, 2010.

[21] M. Barut, R. Demir, E. Zerdali, R. Inan, "Real-time implementation of bi input-extended Kalman filter-based estimator for speed-sensorless control of induction motors", IEEE Transactions on Industrial Electronics, Vol. 59, pp. 4197–4206, 2012.

[22] M. Barut, "Bi-input extended Kalman filter based speed-sensorless vector control of induction motors with the estimations of rotor and stator resistances, load torque, and inertia", ELECTRIMACS Conference Records, 2011 (on CD).

[23] L.C. Zai, C.L. DeMarco, T.A. Lipo, "An extended Kalman filter approach to rotor time constant measurement in PWM induction motor drives", IEEE Transactions on Industry Applications, Vol. 28, pp. 96–104, 1992.

[24] R.S. Pena, G. M. Asher, "Parameter sensitivity studies for induction motor parameter identification using extended Kalman filter", Proceedings of the 5th European Conference on Power Electronics and Applications, Vol. 4, pp. 306–311, 1993.

[25] T. Kataoka, S. Toda, Y. Sato, "On-line estimation of induction motor parameters by extended Kalman filter", Proceedings of the European Conference on Power Electronics and Applications, Vol. 4, pp. 325–329, 1993.

[26] D.H. Choi, M.H. Shin, T.K. Lee, S.B. Cho, D.S. Hyun, "Vector control of an induction motor for the field weakening region with tuning of the magnetizing inductance", Proceedings of the Power Conversion Conference, Vol. 1, pp. 107–112, 1997.

[27] M. Barut, "Extended Kalman filter design and application for sensorless high performance control of squirrel cage induction motors", PhD, İstanbul Technical University Graduate School of Science, Engineering, and Technology, İstanbul, Turkey, 2005 (in Turkish).

[28] P. Vas, Sensorless Vector and Direct Torque Control, Oxford, UK, Oxford University Press, 1998.

[29] B.K. Bose, Modern Power Electronics and AC Drives, Upper Saddle River, NJ, USA, Prentice Hall, 2002.